

## Article

# A W-Band Chebyshev Waveguide Bandpass Filter with Wide Stopband Performance

Zhongbo Zhu <sup>1,2</sup>, Weidong Hu <sup>1,\*</sup>, Kaida Xu <sup>3</sup>, Yuming Bai <sup>1</sup> and Sheng Li <sup>2</sup>

<sup>1</sup> Beijing Key Laboratory of Millimeter Wave and Terahertz Technology, Beijing Institute of Technology, Beijing 100081, China; zhuzb@cast504.com (Z.Z.); bym@bit.edu.cn (Y.B.)

<sup>2</sup> National Key Laboratory of Science and Technology on Space Microwave, China Academy of Space Technology, Xi'an 710100, China; lisheng\_cast@163.com

<sup>3</sup> School of Information and Communications Engineering, Xi'an Jiaotong University, Xi'an 710049, China; kaidaxu@xjtu.edu.cn

\* Correspondence: hoowind@bit.edu.cn

**Abstract:** In this paper, a W-band waveguide bandpass filter with a standard fourth-order Chebyshev response is proposed based on the computer numerical control (CNC)-milling technology. The harmonics-staggered technique and orthogonal coupling method are incorporated into this waveguide filter design without increasing the complexity of the filter structure in order to suppress the intrinsic spurious responses near the passband. Furthermore, the proposed filter design maintains a simple construction, which can be conveniently fabricated using CNC milling. The fabricated waveguide filter exhibits an average insertion loss of 0.9 dB and a return loss of above 20 dB in a 3 dB fractional bandwidth (FBW) of 5.5% centered at 85 GHz. The excellent spurious suppression property can reach better than  $-25$  dB up to 165 GHz. The wide stopband performance of the proposed W-band filter is very competitive compared with the reported waveguide filters.

**Keywords:** bandpass filter; Chebyshev response; CNC milling; spurious suppression; waveguide filter; W-band; wide stopband



**Citation:** Zhu, Z.; Hu, W.; Xu, K.; Bai, Y.; Li, S. A W-Band Chebyshev Waveguide Bandpass Filter with Wide Stopband Performance. *Electronics* **2024**, *13*, 1793. <https://doi.org/10.3390/electronics13091793>

Academic Editors: Niamat Hussain, Sotirios K. Goudos, Felipe Jiménez, Francisco Falcone and Sandra Costanzo

Received: 12 April 2024

Revised: 2 May 2024

Accepted: 4 May 2024

Published: 6 May 2024



**Copyright:** © 2024 by the authors. Licensee MDPI, Basel, Switzerland. This article is an open access article distributed under the terms and conditions of the Creative Commons Attribution (CC BY) license (<https://creativecommons.org/licenses/by/4.0/>).

## 1. Introduction

Millimeter-wave (mmWave) and terahertz (THz) bands have been widely used for various areas including wireless communications [1], imaging radars [2], radio astronomy [3] and atmospheric science [4]. For instance, wireless communication around 100 GHz, which can offer the potential for massive data rates and broad bandwidth, has attracted considerable attention for beyond 5G and 6G communications [1,5]. The interest in modern mmWave and THz communication systems and spectrum detectors has enabled a great demand for abundant active and passive devices, such as oscillators [6], multipliers [7], mixers [8], on-chip amplifiers [9], antenna arrays [10] and filters [11]. Filters, as one of the key devices, can play an invaluable role in most systems, blocking unwanted or spurious waves [12]. It is remarkable that the W-band from 75 to 110 GHz is an important frequency window spectrum for multi-domain applications. Therefore, fast-developing wireless communication systems at the W-band have driven a growing demand for bandpass filters (BPFs) with high performance, such as low loss, high out-of-band rejection and wide stopband.

Numerous mmWave and THz BPFs based on metamaterials, photonic crystals and meshes have been reported [13], but they are exclusively selecting free-space waves in quasi-optical systems. Compared with the substrate-based transmission lines such as substrate-integrated waveguide (SIW) [14,15], microstrip line [16] and coplanar waveguide (CPW) [17], the air-filled rectangular waveguide can exhibit advantages of low insertion loss, high Q-factor, high power handling, and simple assembling. Thus, rectangular waveguides are preferred as the transmission lines to construct BPFs [18–27], active circuits [7–9]

as well as systems [2] from the *W*-band to THz band. However, the physical dimensions suffer from high precision requirements due to short wavelength and small size of the *W*-band BPFs. Therefore, a new generation of micro-machining technologies with high precision has been applied to realize *W*-band waveguide filters, such as the deep reactive ion etching (DRIE) [18], wet etching [19], 3D printing [20], electro-forming [21], and thick SU-8 photoresist technology [22]. Although the micro-machining can manufacture waveguide components operating at higher frequencies [23], currently, expensive clean-room, additional metal fixtures and connections are required, which will make them cost effective only for large-scale array systems. Actually, most solid-state systems in the short-wavelength band are adopting waveguides for main circuitry blocks in combination with lithographic chips [2,7–9]. Thus, the most popular method for producing waveguide components is still the computer numerical control (CNC) milling technique using a split-block way. This technology can strengthen physical robustness while simplifying the assembling and inter-connection, such as the *W*-band filters in [24–31]. In addition, the cross-coupling, extracted poles and high-order modes have been introduced to achieve the advanced quasi-elliptical filtering responses [26–31].

In modern wireless communication systems, the presence of multiple signal frequencies can significantly degrade the communication quality of the overall system. Moreover, spurious signals and harmonics within RF components can adversely affect the performance of mixers and receivers. Therefore, it is essential to develop waveguide BPFs with superior stopband suppression capabilities to address these challenges. However, spurious bands caused by the intrinsic harmonics of waveguide resonators always exist, resulting in poor and narrow upper stopband performance. In the microwave band, a variety of designs have been presented to improve the stopband performance for waveguide filters such as cascading lowpass filters [32–36]. However, these methods cannot be directly scaled up to the *W*-band waveguide filters because of the structure complexity [32,33] and multi-order cavities [36].

In this article, a *W*-band Chebyshev waveguide BPF with excellent stopband suppression performance is designed. The method of controlling both harmonics and couplings is used to realize the extended stopband in the *D*-band. In addition, the proposed fourth-order waveguide BPF can be easily implemented by the CNC milling technique, maintaining a low-loss feature.

## 2. Spurious Suppression Methods

This section discusses two methods for the spurious suppression of waveguide BPF based on the coupling resonator cavities.

### 2.1. Harmonic-Staggered Method

For most waveguide filter designs [18–31], the fundamental  $TE_{101}$  mode is generally considered to construct the filter passband. Each resonator cavity can support multiple harmonic resonances due to high-order modes; however, it will lead to introducing undesired passbands [21,36]. The equivalent circuit diagram is shown in Figure 1, where it considers the dominant passband and spurious passbands. Usually, the high-order resonant modes such as  $TE_{102}$ ,  $TE_{201}$  or  $TE_{103}$  are regarded for coupling to the spurious passbands. Therefore, the idea for breaking spurious passbands to improve stopband performance is mainly focusing on the control of the harmonic modes or the coupled mechanism. As shown in Figure 1, the first way is staggering the intrinsic high-order harmonics, which are marked as the purple symbol “×”.

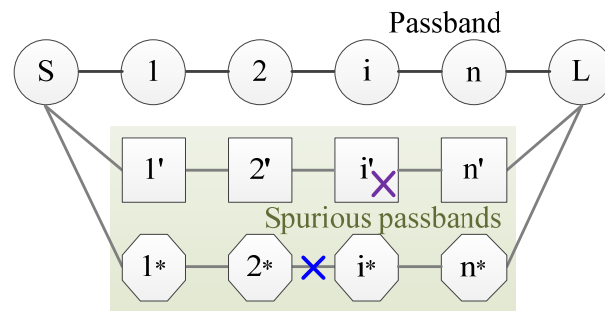


Figure 1. Equivalent circuit diagram considering spurious passbands of the filter.

For a resonator cavity with a size of  $a \times b \times l$ , the  $TE_{101}$  and  $TE_{m0n}$  modes can be calculated by the following equations,

$$f_{TE_{101}} = \frac{c_0}{2} \sqrt{\left(\frac{1}{a}\right)^2 + \left(\frac{1}{l}\right)^2} \dots f_{TE_{m0n}} = \frac{c_0}{2} \sqrt{\left(\frac{m}{a}\right)^2 + \left(\frac{n}{l}\right)^2} \quad (1)$$

where  $a$  and  $l$  are the width and length of the cavity along the  $x$ -axis and  $y$ -axis, respectively. Following (1), the first harmonic passband is usually generated by the  $TE_{102}$  or  $TE_{201}$  mode. Constructions with different ratios of  $a$  to  $l$  can be controlled to obtain staggered high-order harmonics, i.e., different  $f_{TE_{m0n}}$ . Accordingly, Figure 2 gives the normalized frequency distributions of several high-order modes ( $TE_{m0n}$ ) and the fundamental mode  $f_0$  ( $TE_{101}$ ) in two different cavities. The constitutive resonators are selected at the points of  $ratio = 1.38$  and  $ratio = 1.58$ , where  $ratio = f_{TE_{102}} / f_{TE_{101}}$  is defined as the frequency  $ratio$  of the second resonance mode to the fundamental one. It can be seen that the harmonic resonances between  $f_{TE_{101}}$  and  $f_{TE_{202}}$  are irregularly distributed on the frequency spectrum for these two types of resonators. The equation  $f_{TE_{202}} = 2 \cdot f_{TE_{101}}$  is always correct for all resonators in the filter design.

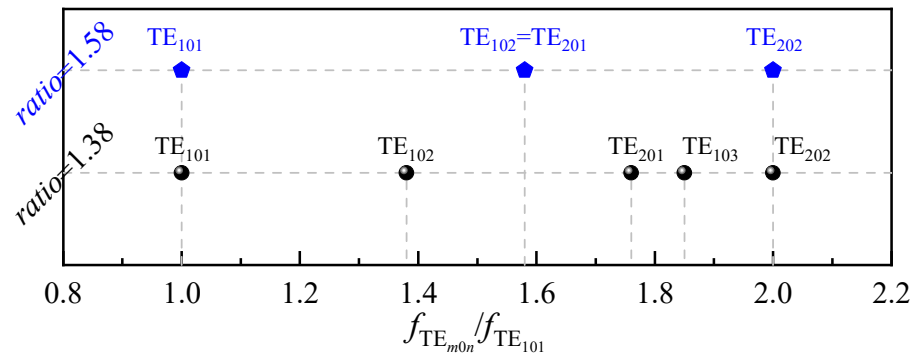
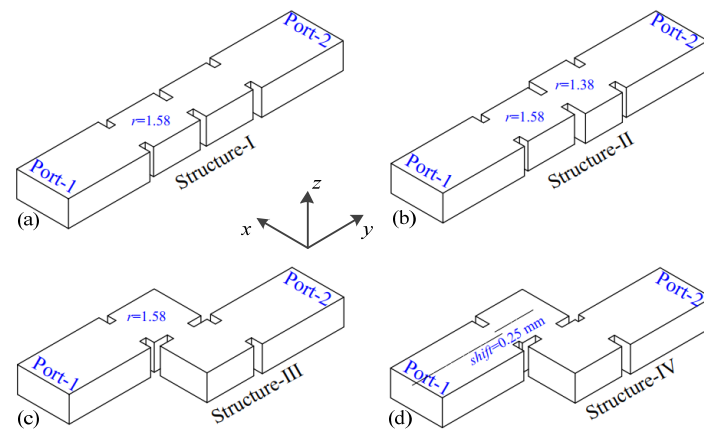
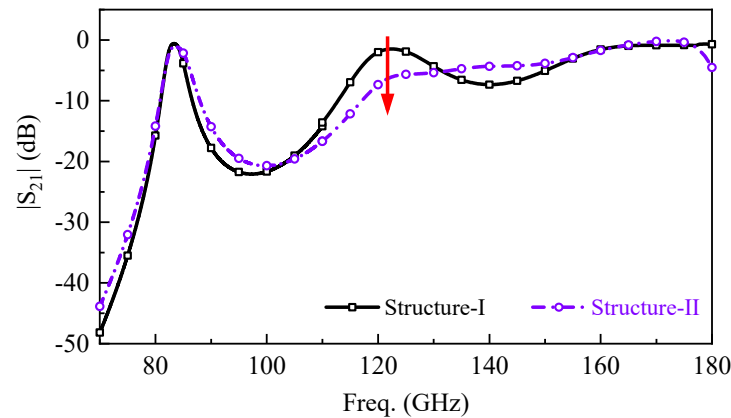


Figure 2. Normalized frequency distributions of several high-order modes in two cavities with ratio = 1.38 and ratio = 1.58.

In order to verify the effectiveness of the above discussed harmonic-staggered technology, Structure-I with two resonators of ratio = 1.58 as well as Structure-II with one resonator of ratio = 1.58 and the other resonator of ratio = 1.38 are constructed, as shown in Figure 3a,b, respectively. Figure 4 illustrates the frequency response comparisons of Structure-II with Structure-I, where the amplitude of the first spurious passband caused by the  $TE_{102}/TE_{201}$  mode can be suppressed by about 6 dB.



**Figure 3.** (a) Structure-I: BPF using two identical coupled square resonator cavities; (b) Structure-II: BPF using two different coupled resonator cavities with ratio = 1.38 and ratio = 1.58, respectively; (c) Structure-III: BPF using two coupled square resonator cavities with orthogonal coupling ports; (d) Structure-IV: BPF using two coupled square resonator cavities with orthogonal coupling ports and offset.



**Figure 4.** Response comparison of Structure-II with Structure-I in Figure 3.

## 2.2. Harmonic-Coupling Control Scheme

The second effective method is to break or modify the coupling paths of harmonics to eliminate spurious passbands. The coupling coefficient between resonators depends on the strength of the tangential component of magnetic field or the normal component of electric field [12]. The magnetic field distributions of the first four modes ( $TE_{101}$ ,  $TE_{102}$ ,  $TE_{201}$  and  $TE_{202}$ ) in a square resonator cavity with a ratio = 1.58 are simulated by Ansys HFSS, as shown in Figure 5. For the  $TE_{101}$  mode, there are four regions with the strongest magnetic field ( $H_x$  and  $H_y$ ) in the middle of all edges. For the higher mode  $TE_{102}$  or  $TE_{201}$ , the maximum magnetic field only appears along the  $x$ - or  $y$ -direction, and the minimum magnetic field occurs along the edge of the  $x$ - or  $y$ -direction, as clearly displayed in Figure 5. Accordingly, by means of the orthogonal couplings, neither the  $TE_{102}$  mode nor  $TE_{201}$  mode can be effectively excited. This property can be confirmed by the simulation of the Structure-III model presented in Figure 3c. Figure 6 illustrates the frequency response comparison of Structure-III with Structure-I. It is seen that the first spurious passband caused by the  $TE_{102}$  or  $TE_{201}$  mode can be greatly suppressed at the specific frequency, but the spurious passband response cannot be eliminated, which is just moved to higher frequency. Additional multiple resonators should be employed to completely eliminate the spurious passband [32], but it will increase the overall insertion loss at the working frequencies.

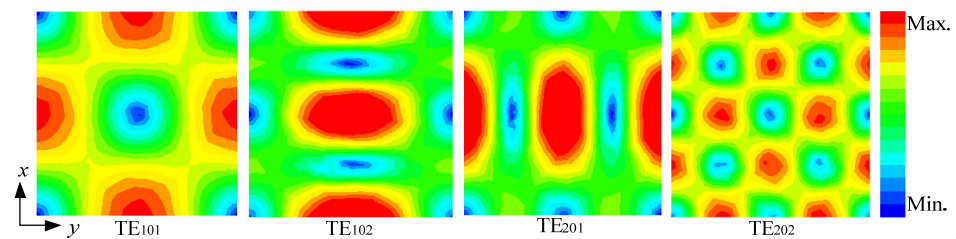


**Figure 5.** Simulated magnetic-field magnitude distributions of the first four modes including TE<sub>101</sub>, TE<sub>102</sub>, TE<sub>201</sub> and TE<sub>202</sub> in a square resonator cavity.

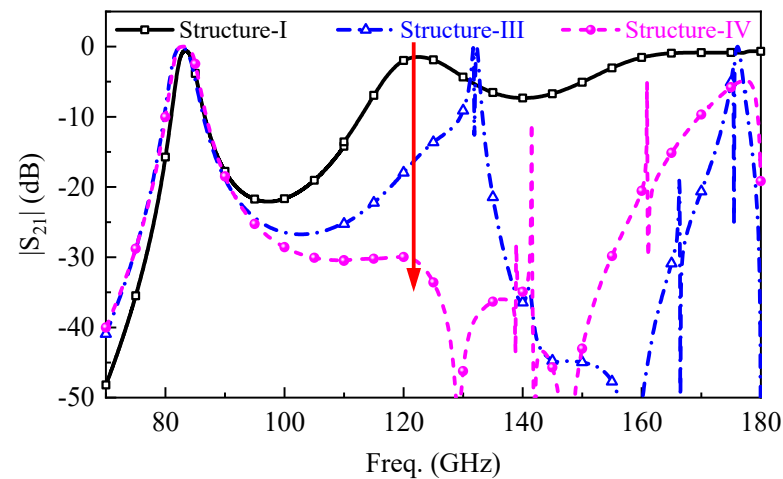


**Figure 6.** Response comparisons of Structure-III and Structure-IV with Structure-I in Figure 3.

There is a more practical approach for fully suppressing spurious passbands based on the orthogonal architecture design [37]. The asymmetry between TE<sub>102</sub> and TE<sub>201</sub> modes after coupling addition can be compensated by moving orthogonal ports away from the middle position with a slight shift, as shown in Figure 3d. From the response comparison of Structure-I, -III and -IV in Figure 6, it is evidently clear that the first spurious passband around 120 GHz can be significantly suppressed to exhibit much better stopband performance. It is worth noting that some other harmonics at higher than  $1.5f_0$  frequencies still exist.

### 3. Filter Design

In this section, a fourth-order waveguide filter with a symmetrical Chebyshev in the W-band is developed to verify the usefulness of the above-mentioned spurious passband suppression methods in improving the stopband performance, according to the following specifications:

- (1) Center frequency  $f_0 \approx 85$  GHz (W-band);
- (2) 3 dB bandwidth FBW  $\approx 5\%$ ;
- (3) In-band return loss better than  $-20$  dB;
- (4) Very wide out of band up to  $2f_0$ .

As shown in Figure 7, this geometric configuration of the W-band filter comprises two standard WR-10 waveguides ( $a \times b = 2.54$  mm  $\times$  1.27 mm), two cavities with ratio = 1.38 (Resonator-1 and Resonator-4) and two resonators with ratio = 1.58 (Resonator-2 and Resonator-3). Obviously, the first strategy is employing four resonators with different ratios to stagger the high-order harmonics to destroy the spurious passbands. The second strategy is using the folded structure to form the orthogonal couplings to decrease the unwanted TE<sub>102</sub> nor TE<sub>201</sub>-mode responses and meanwhile obtain a compact structure, as revealed in Figure 7. The adjacent resonators, namely Resonator-1 and -2, Resonator-2 and -3 and Resonator-3 and -4, are directly magnetic couplings, which are implemented by the classical *H*-plane irises. It should be noted that there are no cross-couplings in this

filter; as a result, a typical Chebyshev response will be obtained [12]. The third strategy is shifting certain couplings to compensate coupling orthogonality to completely eliminate the spurious passbands from the  $f_0$  to  $2f_0$  band. In this design, the couplings between the input waveguide and Resonator-1, Resonator-2 and 3, as well as Resonator-4 and the output waveguide are shifted, as indicated in Figure 7. All the vertical corners have been filleted with a 0.2 mm radius (R), which is necessary for such a high-frequency filter considering the non-negligible drill size, as shown in Figure 7. Therefore, the previously discussed methods including the harmonics-staggered technique and orthogonal coupling method have been incorporated into this waveguide filter design without increasing the complexity and difficulty of the structure.

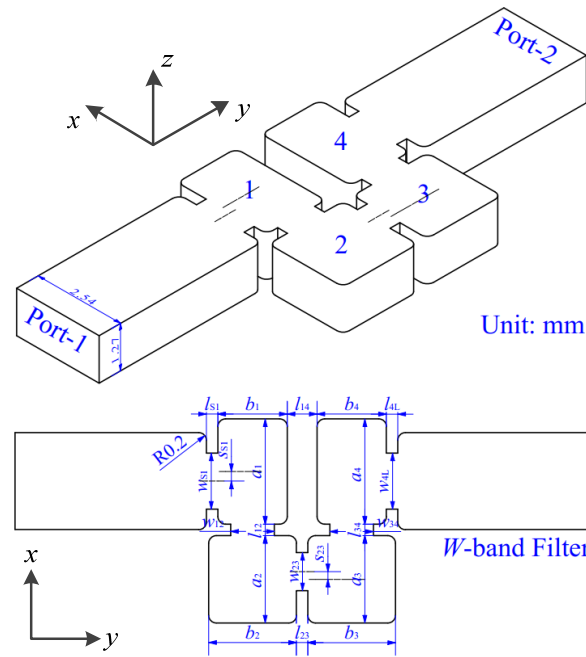


Figure 7. Three-dimensional (3D) and top view of the W-band waveguide filter.

Several structural ways have been used in this design, while no other theory would be involved. Therefore, this filter design can be realized by using the well-illustrated coupling matrix method [12,38,39]. Based on the above specifications, the coupling coefficients of this W-band filter can be synthesized in Table 1 and then be transformed into physical dimensions according to the procedure. Thus, most of the initial parameters of this filter can be acquired. In the last step, the shift value would be conveniently obtained using the commercial simulator ANSYS HFSS while all the other parameters are kept unchanged. The final step is only used to improve the stopband performance, while the variation in passband is almost negligible.

Table 1. Coupling coefficients of the proposed Chebyshev filter.

|                      | $M_{S1}$ | $M_{12}$ | $M_{23}$ | $M_{34}$ | $M_{4L}$ |
|----------------------|----------|----------|----------|----------|----------|
| Coupling coefficient | 0.0674   | 0.061    | 0.045    | 0.061    | 0.0674   |

After a fine-tuning optimization procedure in ANSYS HFSS, the final dimensions of the proposed W-band waveguide filter are tabulated in Table 2. The proposed W-band waveguide filter was fabricated in an aluminum (Al) block based on the H-plane split method by the CNC-milling technology, as shown in Figure 8. The whole filter structure was machined within one block to avoid the problems of misalignment and high aspect ratio. The minimum radius of drills during the milling process is 0.2 mm, which has been taken into account in the simulation. The assembled Al block has a volume

of  $W \times L \times H = 20 \times 20 \times 20 \text{ mm}^3$ , as shown in Figure 8a. Figure 8b gives the top view microphotograph of the internal structure, where it can be seen that both the fineness and flatness are achieved to guarantee a good electrical contact.

**Table 2.** Parameter values of the proposed Chebyshev filter.

| Para. | Value | Para.    | Value | Para.    | Value    | Para.    | Value    |
|-------|-------|----------|-------|----------|----------|----------|----------|
| $a$   | 2.54  | $a_3$    | $a_1$ | $w_{12}$ | 1.14     | $L_{14}$ | 0.78     |
| $b$   | 1.27  | $l_3$    | $l_1$ | $l_{12}$ | 0.3      | $w_{4L}$ | $w_{S1}$ |
| $a_1$ | 2.76  | $a_4$    | $a_2$ | $w_{23}$ | 1.0      | $l_{4L}$ | $l_{S1}$ |
| $l_1$ | 1.81  | $l_4$    | $l_2$ | $l_{23}$ | 0.3      | $s_{S1}$ | 0.25     |
| $a_2$ | 2.29  | $w_{S1}$ | 1.47  | $w_{34}$ | $w_{12}$ | $s_{23}$ | 0.2      |
| $l_2$ | $a_2$ | $l_{S1}$ | 0.3   | $l_{34}$ | $l_{12}$ | $R$      | 0.2      |

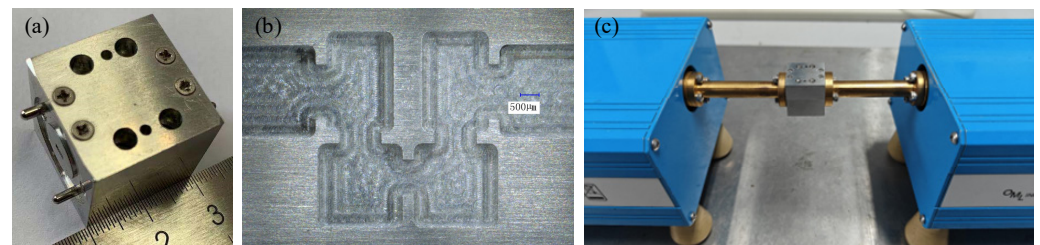


**Figure 8.** (a) Photograph, (b) top view photomicrograph of inside of the fabricated filter and (c) the measurement setup.

#### 4. Simulation and Measurement Results

The final simulated frequency response is shown in Figure 9 (dot dash line). It is clear that a significant wide stopband from  $f_0$  to  $2f_0$  is obtained through such design. The spurious response suppression of better than  $-25 \text{ dB}$  is greatly improved and the first spurious appears at about  $165 \text{ GHz}$ , which is twice that of the center frequency ( $2f_0$ ). This waveguide filter has a standard Chebyshev response with a  $3 \text{ dB}$  fractional bandwidth (FBW) of  $5.5\%$  in the  $W$ -band. Measurements of the fabricated filter were carried out by the Agilent PNA-X vector network analyzer (VNA) connecting with frequency extension modules of  $75\text{--}110 \text{ GHz}$  and  $110\text{--}170 \text{ GHz}$ , as shown in Figure 8c. The through-reflect-line (TRL) calibration was first implemented, and then the packaged block was connected and fixed to the standard waveguide converters through UG-387 flanges for measurement.

The tested and simulated S-parameter results of this  $W$ -band filter are compared in Figure 9. Very good agreement between the simulations and measurements including the passband and stopband performance is observed. It can be seen from the measured results that this practical filter can provide excellent spurious suppression with  $-25 \text{ dB}$  up to  $2f_0$ . The original parasitic bands that resulted from harmonic modes between  $f_0$  and  $2f_0$  have been completely eliminated. Consequently, this filter exhibits outstanding stopband performance without introducing additional resonators, structures or losses.

In addition, as can be seen in the detailed performance in the  $75\text{--}100 \text{ GHz}$  band in Figure 10, the basically symmetrical Chebyshev response has been achieved. The simulated  $3 \text{ dB}$  FBW is about  $5.5\%$  from  $83.1$  to  $87.8 \text{ GHz}$ , whereas the measured  $3 \text{ dB}$  FBW is about  $5.5\%$  from  $82.5$  to  $87.2 \text{ GHz}$ . They are matched well with the exception of a small band shift of about  $0.6 \text{ GHz}$  (i.e.,  $0.7\% \cdot f_0$ ) toward low frequency, which might be due to the machining, assembly or measurement errors. The measured return loss (RL) is better than  $20 \text{ dB}$ , which is degraded slightly compared to the simulation. As shown in the bottom subfigure of Figure 10, both the actual and expected losses are at the same level in the passband. An insertion loss of about  $0.9 \text{ dB}$  has been achieved for this filter prototype. The value of  $3.5 \times 10^6 \text{ S/m}$  as the equivalent conductivity has been discussed in [26,27,40],

which can include multiple effects of non-ideal metallic conductors, surface roughness, electric contact, as well as other possible issues during the machining, assembling and testing process. Of course, the IL performance can be further improved by gold or copper plating within the block.

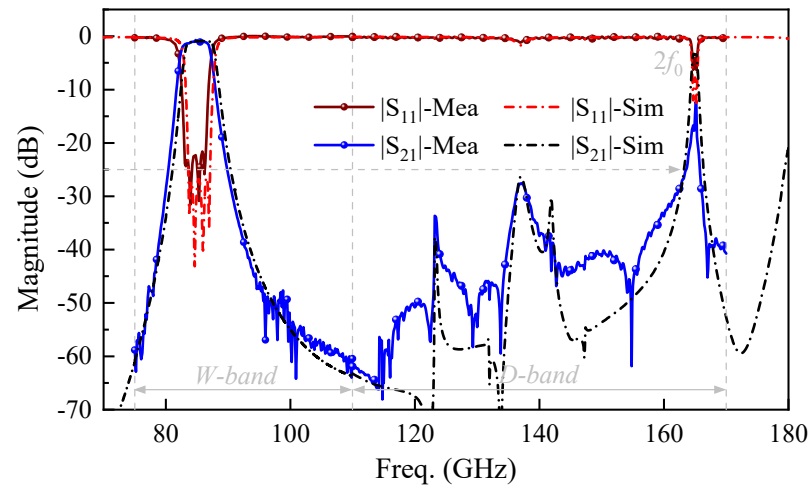


**Figure 9.** Simulated and measured results of this filter in the wideband of 75–170 GHz. An equivalent conductivity of  $3.5 \times 10^6$  S/m is used in the simulation.

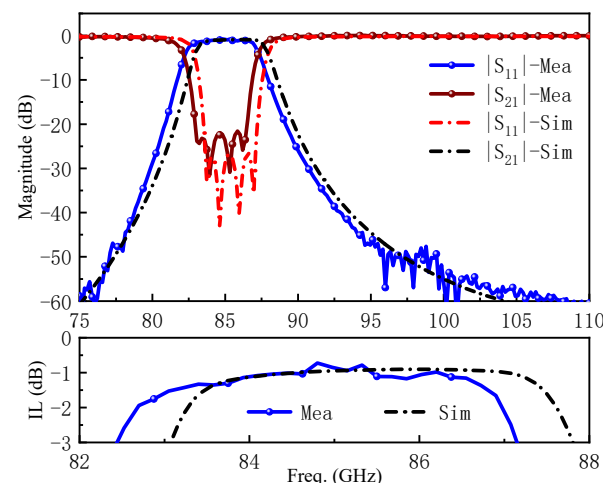


**Figure 10.** The detailed performance of this filter in full W-band.

Table 3 gives the performance summary of the recently reported W-band waveguide filters compared to our work. Most filters [18–22] have exhibited high performance, such as low loss, multiple transmission zeros and wide passband, except SIW filters [14,15] with high dielectric losses. As can be observed from Table 3, the performance including the low orders, passband width, IL and RL of our filter is comparable with the most advanced W-band filters [14,15,18–31]. Although there is no transmission zero in this filter design, the standard Chebyshev response with sharp side-bands has also been obtained, which benefits from the spurious-free response nearby the passband. This proposed waveguide filter has achieved a high rejection property out of band, especially in the wide upper stopband, and it outperformed other classical filters in such a W-band. The aforementioned results have also indicated that our proposed filter can be absolutely suitable through the CNC-machining fabrication while maintaining high performance.

**Table 3.** Performance summary of W-band waveguide filters based on different technologies.

| Ref.            | Center Frequency | Filter Order | No. of TZs | 3 dB FBW | IL/dB (Average) | RL/dB | Stopband Suppression                            | Technology                   |
|-----------------|------------------|--------------|------------|----------|-----------------|-------|---|------------------------------|
| [14]            | 80 GHz           | 4            | 1          | 2.5%     | 3.9             | 10    | No  | PCB-based SIW                |
| [15]            | 93 GHz           | 4            | 2          | 3.4%     | 4.3             | 13.5  | No  | GaAs-based SIW               |
| [18]            | 93.7 GHz         | 4            | —          | 4.9%     | 1.3             | 16    | No  | DRIE                         |
| [19]            | 94 GHz           | 2            | —          | 1.3%     | 1.75            | 15    | No  | Wet-etching                  |
| [20]            | 100 GHz          | 4            | —          | 4%       | 0.8             | 15    | No  | Laser Micromachining         |
| [20]            | 87.5 GHz         | 4            | —          | 11.5%    | 0.5             | 18    | No  | 3D-printing                  |
| [21]            | 90 GHz           | 10           | —          | 20%      | 0.4             | 15    | 10th-order, 1st spurious@ $1.5f_0$              | Electroforming               |
| [22]            | 100 GHz          | 4            | 2          | 5%       | 1.2             | 10    | No  | SU-8 Photoresist             |
| [24]            | 91.3 GHz         | 5            | —          | 20%      | 0.6             | 15    | No  | Offset-coupling, CNC         |
| [25]            | 100 GHz          | 4            | —          | 6%       | 0.5             | 13    | No  | TM <sub>120</sub> -mode, CNC |
| [26]            | 92.6 GHz         | 4            | 4          | 5.5%     | 1.2             | 15    | No  | Cross-coupling, CNC          |
| [27]            | 100 GHz          | 4            | 1          | 10%      | 0.6             | 18    | No  | Extracted pole, CNC          |
| [29]            | 88.55 GHz        | 2            | 3          | 3.6%     | 1.15            | 18    | No  | PCB, CNC                     |
| [30]            | 90 GHz           | 4            | 2          | 7.3%     | 0.63            | 20    | No  | TM-mode, CNC                 |
| Proposed Filter | 85 GHz           | 4            | —          | 5.5%     | 0.9             | 20    | Yes, better than $-25$ dB, 1st spurious@ $2f_0$ | CNC                          |

In the near future, waveguide BPFs working at the W-band and above will be developed toward multiple passbands with a wider stopband. In addition, the environmental experiments including wide adaptable temperature and mass manufacturing should be explored for further design of the waveguide filter. It will provide a deeper insight into the practical development and applications of the proposed W-band BPF.

## 5. Conclusions

A W-band waveguide filter with wide stopband performance has been proposed and evaluated based on the CNC-milling technology. The intrinsic spurious responses from  $f_0$  to  $2f_0$  can be fully eliminated using multiple spurious passband suppression methods. High performance including the standard Chebyshev response with a low IL of 0.9 dB in the W-band and excellent stopband rejection level of  $-25$  dB have been achieved. Such a method can be even scaled up to the THz frequency band by using the advanced CNC-milling or micro-machining technologies. It is of great potential for the applications in millimeter-wave and THz waveguide components and systems.

**Author Contributions:** Conceptualization, Z.Z. and K.X.; methodology, Z.Z. and K.X.; software, Z.Z.; validation, Z.Z.; formal analysis, Z.Z., W.H., Y.B. and S.L.; investigation, Z.Z.; writing—original draft preparation, Z.Z. and K.X.; writing—review and editing, K.X.; supervision, W.H. and K.X. All authors have read and agreed to the published version of the manuscript.

**Funding:** This work was supported in part by the NSAF Joint Fund under Grant U2130102, and in part by the “Siyuan Scholar” Fellowship of XJTU.

**Data Availability Statement:** The data presented in this study are available on request from the corresponding author.

**Conflicts of Interest:** The authors declare no conflicts of interest.

## References

- Giordani, M.; Polese, M.; Mezzavilla, M.; Rangan, S.; Zorzi, M. Toward 6G networks: Use cases and technologies. *IEEE Commun. Mag.* **2020**, *58*, 55–61. [\[CrossRef\]](#)
- Cooper, K.B.; Chattopadhyay, G. Submillimeter-wave radar: Solid-state system design and applications. *IEEE Microw. Mag.* **2014**, *15*, 51–67. [\[CrossRef\]](#)
- Kulesa, C. Terahertz spectroscopy for astronomy: From comets to cosmology. *IEEE Trans. Terahertz Sci. Technol.* **2011**, *1*, 232–240. [\[CrossRef\]](#)

4. Li, S.; Yao, Q.; Liu, D.; Duan, W.; Zhang, K.; Jin, J.; Lin, Z.; Wu, F.; Yang, J.; Miao, W.; et al. Terahertz superconducting radiometric spectrometer in Tibet for atmospheric science. *J. Infrared Millim. Terahertz Waves* **2019**, *40*, 166–177. [[CrossRef](#)]
5. IAKyildiz, F.; Kak, A.; Nie, S. 6G and beyond: The future of wireless communications systems. *IEEE Access* **2020**, *8*, 133995–134030. [[CrossRef](#)]
6. Li, X.; Wang, J.; Sun, J.; Song, Z.; Ye, H.; Zhang, Y.; Zhang, L. Experimental study on a high-power subterahertz source generated by an overmoded surface wave oscillator with fast startup. *IEEE Trans. Electron. Devices* **2013**, *60*, 2931–2935. [[CrossRef](#)]
7. Mehdi, I.; Siles, J.; Lee, C.; Schlecht, E. THz diode technology: Status, prospects, and applications. *Proc. IEEE* **2017**, *105*, 990–1007. [[CrossRef](#)]
8. Peter Westig, M.; Justen, M.; Jacobs, K.; Stutzki, J.; Schultz, M.; Schomacker, F.; Honingh, N. A 490 GHz planar circuit balanced Nb-Al<sub>2</sub>O<sub>3</sub>-Nb quasiparticle mixer for radio astronomy: Application to quantitative local oscillator noise determination. *J. Appl. Phys.* **2012**, *112*, 093919. [[CrossRef](#)]
9. Westig, P.; Klapwijk, M. Josephson parametric reflection amplifier with integrated directionality. *Phys. Rev. Appl.* **2018**, *9*, 064010. [[CrossRef](#)]
10. Zhu, Z.; Hu, W.; Qin, T.; Li, S.; Li, X.; Zeng, J.; Lin, X.; Lighthart, L.P. A high-precision terahertz retrodirective antenna array with navigation signal at a different frequency. *Front. Inform. Technol. Electron. Eng.* **2020**, *21*, 377–383. [[CrossRef](#)]
11. Ding, J.-Q.; Shi, S.-C.; Zhou, K.; Zhao, Y.; Liu, D.; Wu, W. WR-3 band quasi-elliptical waveguide filters using higher order mode resonances. *IEEE Trans. Terahertz Sci. Technol.* **2017**, *7*, 302–309. [[CrossRef](#)]
12. Hong, J.-S.; Lancaster, M.J. *Microstrip Filters for RF/Microwave Applications*; Wiley: New York, NY, USA, 2001.
13. Wang, Y.; Yang, B.; Tian, Y.; Donnan, R.S.; Lancaster, M.J. Micromachined thick mesh filters for millimeter-wave and terahertz applications. *IEEE Trans. Terahertz Sci. Technol.* **2014**, *4*, 247–253. [[CrossRef](#)]
14. Hao, Z.-C.; Ding, W.-Q.; Hong, W. Developing low-cost W-band SIW bandpass filters using the commercially available printed-circuitboard technology. *IEEE Trans. Microw. Theory Tech.* **2016**, *64*, 1775–1786. [[CrossRef](#)]
15. Xiao, Y.; Shan, P.; Zhao, Y.; Sun, H.; Yang, F. Design of a W-band GaAs-based SIW chip filter using higher order mode resonances. *IEEE Microw. Wirel. Compon. Lett.* **2019**, *29*, 104–106. [[CrossRef](#)]
16. Barry, P.S.; Shirokoff, E.; Kovács, A.; Reck, T.J.; Hailey-Dunsheath, S.; McKenney, C.M.; Swenson, L.J.; Hollister, M.I.; Leduc, H.G.; Doyle, S.; et al. Electromagnetic design for SuperSpec, a lithographically-patterned millimeter-wave spectro-graph. *Proc. SPIE* **2012**, *8452*, 738–747.
17. Eblabla, A.M.; Li, X.; Wallis, D.J.; Guiney, I.; Elgaid, K. GaN on low-resistivity silicon THz high-Q passive device technology. *IEEE Trans. Terahertz Sci. Technol.* **2017**, *7*, 93–97. [[CrossRef](#)]
18. Song, S.; Yoo, C.S.; Seo, K.S. W-band bandpass filter using micromachined air-waveguide resonator with current probes. *IEEE Microw. Wirel. Compon. Lett.* **2010**, *20*, 205–207. [[CrossRef](#)]
19. Song, S.; Seo, K.-S. A -band air-cavity filter integrated on a thin-film substrate. *IEEE Microw. Wirel. Compon. Lett.* **2009**, *19*, 200–202. [[CrossRef](#)]
20. Shang, X.; Penchev, P.; Guo, C.; Lancaster, M.J.; Dimov, S.; Dong, Y.; Favre, M.; Billod, M.; de Rijk, E. W-band waveguide filters fabricated by laser micromachining and 3-D printing. *IEEE Trans. Microw. Theory Tech.* **2016**, *64*, 2572–2580. [[CrossRef](#)]
21. Leal-Sevillano, C.A.; Pisano, G.; Montejo-Garai, J.R.; Maffei, B.; Ruiz-Cruz, J.A.; Ng, M.W.; Rebollar, J.M. Development of low loss waveguide filters for radio-astronomy applications. *Infrared Phys. Technol.* **2013**, *61*, 224–229. [[CrossRef](#)]
22. Leal-Sevillano, C.A.; Montejo-Garai, J.R.; Ke, M.; Lancaster, M.J.; Ruiz-Cruz, J.A.; Rebollar, J.M. A pseudo-elliptical response filter at W-band fabricated with thick SU-8 photo-resist technology. *IEEE Microw. Wirel. Compon. Lett.* **2012**, *22*, 105–107. [[CrossRef](#)]
23. Chattopadhyay, G.; Reck, T.; Lee, C.; Jung-Kubiak, C. Micromachined packaging for terahertz systems. *Proc. IEEE* **2017**, *105*, 1139–1150. [[CrossRef](#)]
24. Xu, J.; Ding, J.-Q.; Zhao, Y.; Ge, J.-X. W-band broadband waveguide filter based on H-plane offset coupling. *J. Infrared Millim. Terahertz Waves* **2019**, *40*, 412–418. [[CrossRef](#)]
25. Shang, X.; Lancaster, M.; Dong, Y.-L. W-band waveguide filter based on large TM<sub>120</sub> resonators to ease CNC milling. *IET Electron. Lett.* **2017**, *53*, 488–490. [[CrossRef](#)]
26. Ding, J.; Liu, D.; Shi, S.C.; Wu, W. W-band quasi-elliptical waveguide filter with cross-coupling and source-load coupling. *Electron. Lett.* **2016**, *52*, 1960–1961. [[CrossRef](#)]
27. Leal-Sevillano, C.A.; Montejo-Garai, J.R.; Ruiz-Cruz, J.A.; Rebollar, J.M. Low-loss elliptical response filter at 100 GHz. *IEEE Microw. Wirel. Compon. Lett.* **2012**, *22*, 459–461. [[CrossRef](#)]
28. Liu, Y.; Xu, K.-D.; Li, J.; Guo, Y.-J.; Zhang, A.; Chen, Q. Millimeter-wave E-plane waveguide bandpass filters based on spoof surface plasmon polaritons. *IEEE Trans. Microw. Theory Tech.* **2022**, *70*, 4399–4409. [[CrossRef](#)]
29. Jiang, Y.; Huang, Z.-Y.; Liu, B.-Y.; Zhang, X.-F.; Wang, C.; Wu, W.-W.; Yuan, N.-C. W-band E-plane waveguide filter using compact beeline resonator. *IEEE Microw. Wirel. Compon. Lett.* **2022**, *32*, 289–292. [[CrossRef](#)]
30. Bartlett, C.; Bornemann, J.; Höft, M. Improved TM dual-mode filters with reduced fabrication complexity. *IEEE J. Microw.* **2023**, *3*, 60–69. [[CrossRef](#)]
31. Xu, K.-D.; Xia, S.; Guo, Y.; Cui, J.; Zhang, A.; Chen, Q. W-Band E-plane waveguide bandpass filter based on meander ring resonator. *IEEE Microw. Wirel. Compon. Lett.* **2021**, *31*, 1267–1270. [[CrossRef](#)]
32. Cameron, R.J.; Yu, M.; Wang, Y. Direct-coupled microwave filters with single and dual stopbands. *IEEE Trans. Microw. Theory Tech.* **2005**, *53*, 3288–3297. [[CrossRef](#)]

33. Budimir, D. Optimized E-plane bandpass filters with improved stopband performance. *IEEE Trans. Microw. Theory Tech.* **1997**, *45*, 212–220. [[CrossRef](#)]
34. Morelli, M.; Hunter, I.; Parry, R.; Postoyalko, V. Stopband performance improvement of rectangular waveguide filters using stepped impedance resonators. *IEEE Trans. Microw. Theory Tech.* **2002**, *50*, 1657–1664. [[CrossRef](#)]
35. Zhou, K.; Zhou, C.-X.; Wu, W. Resonance characteristics of substrate-integrated rectangular cavity and their applications to dualband and wide-stopband bandpass filters design. *IEEE Trans. Microw. Theory Tech.* **2017**, *65*, 1511–1524. [[CrossRef](#)]
36. Wu, Q.; Zhu, F.; Yang, Y.; Shi, X. An effective approach to suppressing the spurious mode in rectangular waveguide filters. *IEEE Microw. Wirel. Compon. Lett.* **2019**, *29*, 703–705. [[CrossRef](#)]
37. Chu, P.; Guo, L.; Zhang, L.; Xu, F.; Hong, W.; Wu, K. Wide stopband substrate integrated waveguide filter implemented by orthogonal ports' offset. *IEEE Trans. Microw. Theory Tech.* **2020**, *68*, 964–970. [[CrossRef](#)]
38. Cameron, R.J. Advanced coupling matrix synthesis techniques for microwave filters. *IEEE Trans. Microw. Theory Tech.* **2003**, *51*, 1–10. [[CrossRef](#)]
39. Soto, P.; Tarín, E.; Boria, V.E.; Vicente, C.; Gil, J.; Gimeno, B. Accurate Synthesis and Design of Wideband and Inhomogeneous Inductive Waveguide Filters. *IEEE Trans. Microw. Theory Tech.* **2010**, *58*, 2220–2230. [[CrossRef](#)]
40. Groiss, S. Numerical Analysis of Lossy Cavity Resonators. Ph.D. Thesis, Technical University of Graz, Graz, Austria, June 1996.

**Disclaimer/Publisher's Note:** The statements, opinions and data contained in all publications are solely those of the individual author(s) and contributor(s) and not of MDPI and/or the editor(s). MDPI and/or the editor(s) disclaim responsibility for any injury to people or property resulting from any ideas, methods, instructions or products referred to in the content.